Journal of Pharmacological Sciences 157 (2025) 104–112

Contents lists available at ScienceDirect

Journal of Pharmacological Sciences

journal homepage: www.elsevier.com/locate/jphs

Full paper

Goreisan suppresses cardiac remodeling and dysfunction in a new mouse model with diabetic cardiomyopathy

Masafumi Funamoto [a,*,1], Shunji Hirose [b,1], Mizuho Yamamoto [a], Hai Du Ly-Nguyen [a], Masaki Imanishi [b], Fuka Ebi [b], Mai Ito [b], Hirokazu Ohminami [c], Koichiro Tsuchiya [b], Yasumasa Ikeda [a,**]

[a] Department of Pharmacology, Graduate School of Biomedical Sciences, Tokushima University, Tokushima, Tokushima, Japan
[b] Department of Medical Pharmacology, Graduate School of Biomedical Sciences, Tokushima University, Tokushima, Tokushima, Japan
[c] Department of Clinical Nutrition and Food Management, Graduate School of Biomedical Sciences, Tokushima University, Tokushima, Tokushima, Japan

ARTICLE INFO

Keywords:
Kampo medicine
Diabetic cardiomyopathy
Goreisan
Apoptosis
Oxidative stress

ABSTRACT

Background: The global increase in diabetes, driven by aging populations and lifestyle changes, has led to an increase in the incidence of diabetic cardiomyopathy (DCM). DCM is characterized by metabolic abnormalities, oxidative stress, and inflammation, leading to cardiac remodeling and dysfunction. Goreisan (GRS), a traditional Japanese Kampo medicine, is commonly used to treat fluid control such as edema, due to its diuretic effect. In this study, we examined the effects of GRS on DCM.
Methods: We first established a new mouse model of DCM and then evaluated the effects of GRS on DCM using a recently developed model.
Results: The DCM mouse model developed cardiac hypertrophy, fibrosis, and dysfunction by nine weeks, which was ameliorated by GRS administration. GRS suppressed apoptosis and protein degradation by inhibiting Akt dephosphorylation and oxidative stress in DCM mice. In contrast, no differences in inflammatory cytokine levels were observed, regardless of GRS administration.
Conclusion: GRS has potential efficacy in preventing DCM onset and development.

1. Introduction

The prevalence and the risk of diabetes has been increased worldwide due to the increment of aging population and lifestyle change.[1] Diabetes is a significant risk factor for a number of various complications such as diabetic cardiomyopathy (DCM).[2] DCM is a specific myocardial disorder induced by diabetes and is a major cause of heart failure. Therefore, DCM has a strong impact on the poor prognosis of patients with diabetes, and inadequate diabetes management increases the risk of its development.[3] It is a critical issue in the development of preventive and therapeutic strategies for DCM.

DCM arises from intricate interactions involving metabolic irregularities, oxidative stress, and inflammatory responses associated with hyperglycemia.[4] Notably, abnormalities in protein degradation pathways play a pivotal role in cardiac remodeling.[5] In DCM, the catabolic process is enhanced, leading to increased degradation of myocardial proteins. This process, along with apoptosis, accelerates cardiac remodeling.[6] Cardiac remodeling, which encompasses structural and functional alterations in cardiomyocytes, is a critical step in the progression of cardiomyopathy.[7] In DCM, aberrant protein degradation and apoptosis result in myocardial remodeling, which, in turn, leads to hypertrophy and fibrosis of the myocardium.[8] Cardiac remodeling induced by DCM ultimately causes cardiac dysfunction and increases the risk of heart failure.

Herbal medicines have a long history of playing an important role in the prevention and treatment of complex diseases. These medicines offer a rich source of natural therapeutic compounds and are generally considered effective and safe, with a high level of acceptance as complementary and alternative medicines in Western countries.[9] Goreisan (GRS), a traditional Japanese herbal medicine, is primarily used to

* Corresponding author.
** Corresponding author.
E-mail addresses: funamoto@tokushima-u.ac.jp (M. Funamoto), yasuike@tokushima-u.ac.jp (Y. Ikeda).
[1] MF and SH contributed equally to this study.

https://doi.org/10.1016/j.jphs.2025.01.003
Received 18 September 2024; Received in revised form 29 December 2024; Accepted 3 January 2025
Available online 4 January 2025

Table 1
Primer sequences.

	Forward	Reverse
Mouse atrial natriuretic peptide (*Nppa*)	ATCTGCCCTCTTGAAAAGCA	ACACACCACAAGGGCTTAGG
Mouse brain natriuretic peptide (*Nppb*)	CAGCTCTTGAAGGACCAAGG	AGACCCAGGCAGAGTCAGAA
Mouse collagen type Iα chain (*Col1a1*)	GAGCGGAGAGTACTGGATCG	GCTTCTTTTCCTTGGGGTTC
Mouse tumor necrosis factor-α (*Tnfa*)	ACGGCATGGATCTCAAAGAC	GTGGGTGAGGAGCACGTAGT
Mouse interleukin 1β (*Il1b*)	CAGGCAGGCAGTATCACTCA	TGTCCTCATCCTGCAAGGTC
Mouse interleukin 6 (*Il6*)	CCGGAGAGGAGACTTCACAG	TCCACGATTTCCCAGAGAAC
Mouse gp91^{phox} (*Cybb*)	CAAGATGGAGGTGGGACAGT	GCTTATCACAGCCACAAGCA
Mouse p22^{phox} (*Cyba*)	GTGGACTCCCATTGAGCCTA	CTCCTCTTCACCCTCACTCG
36B4	GCTCCAAGCAGATGCAGCA	CCGGATGTGAGGCAGCAG

improve fluid metabolism by regulating water circulation in the body and promoting diuresis mediated through aquaporin.[10] There have been reports suggesting that GRS might be effective for the heart, with clinical trials investigating its benefits for heart failure.[11] However, there is limited evidence regarding the direct effects of GRS on heart disease such as DCM. This study aimed to evaluate the efficacy of GRS in the treatment of DCM.

2. Materials and methods

2.1. Materials

Ethical Kampo extract formulation (Goreisan) was provided by Tsumura and Co. (Tokyo, Japan). The following commercially available antibodies were used: anti-phospho-Akt (S473), anti-Akt, anti-cleaved caspase-3 (Cell Signaling Technology, MA, USA), anti-transforming growth factor (TGF)-β1, anti-β-actin (Santa Cruz Biotechnology, TX, USA), anti-α-smooth muscle actin (SMA) (Sigma-Aldrich, MO, USA), and anti-4-hydoroxynonenal (HNE) (Bioss Inc., MA, USA).

2.2. Animal experiment procedure

All experimental procedures were performed in accordance with the guidelines of the Animal Research Committee of Tokushima University Graduate School, and the protocol was approved by the Institutional Review Board of Tokushima University Graduate School (approval number: T2022-100). C57BL/6 N male mice (8 weeks old, 22–25 g) were purchased from Japan SLC, Inc. (Shizuoka, Japan). In the control group, mice were fed a normal diet (AIN-93 M, Oriental Yeast Co., Tokyo, Japan) and sterilized water ad libitum for nine weeks, with sterilized water administered orally daily. In the DCM group, the mice were fed a high-fat diet (HFD; HFD-60, Oriental Yeast Co.) (Basal composition: 256.0 g milk casein, 3.6 g L-cystine, 60.0 g maltodextrin, 160.0 g α-corn starch, 55.0 g sucrose, 20.0 g of soybean oil, 330.0 g of lard, 66.1 g of powdered cellulose, 35.0 g of AIN-93G mineral mix, 1.8 g of calcium carbonate, 10.0 g of AIN-93G vitamin mix, and 2.5 g of Choline bitartrate per kilogram of diet) and L-NAME (1 g/L, Nacalai Tesque. Kyoto, Japan) ad libitum for nine weeks. In the 5th week, streptozotocin was administered intraperitoneally at a dose of 50 mg/kg after 4h of starvation for five consecutive days, and sterilized water was administered orally daily. In the DCM + GRS group, mice were fed a HFD and L-NAME ad libitum for 9 weeks. In the 5th week, streptozotocin was administered intraperitoneally at a dose of 50 mg/kg for 5 consecutive days. In

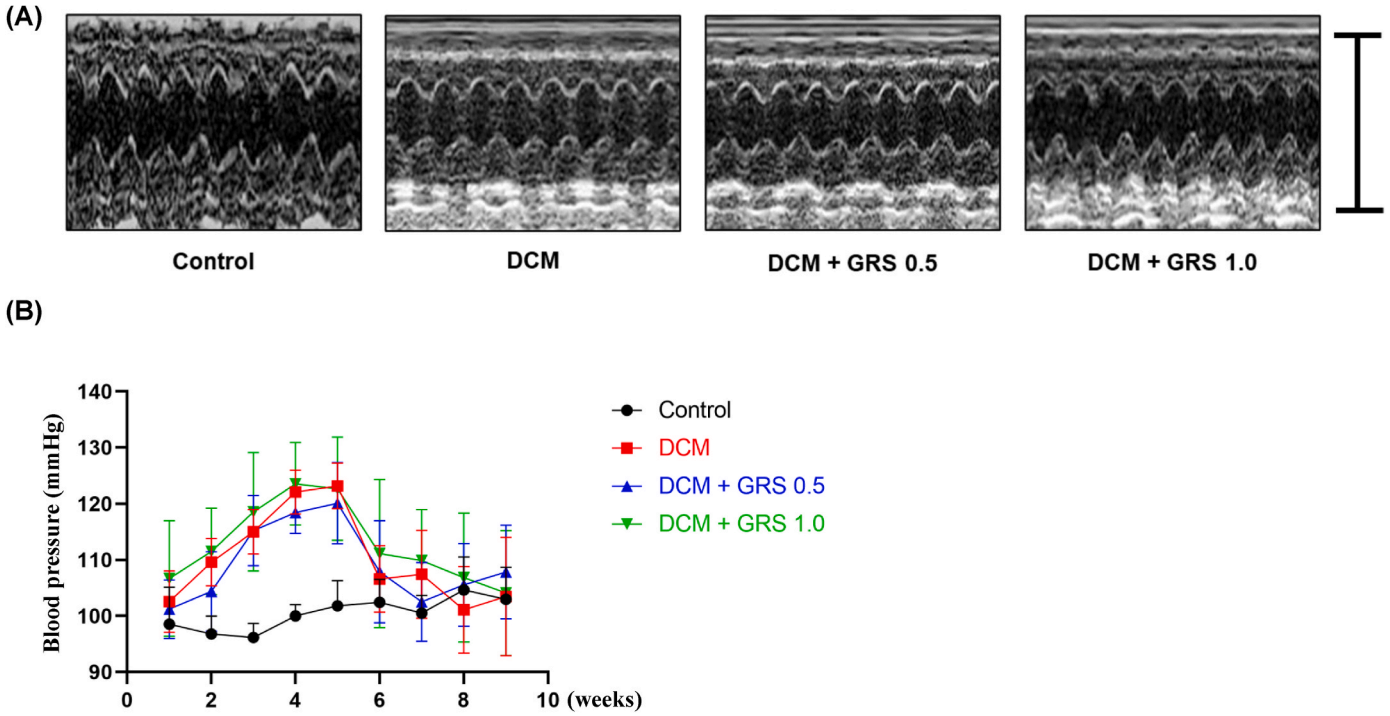

Fig. 1. GRS suppresses cardiac dysfunction in DCM
(A) Representative cardiac echocardiography images from each group. Scale bar: 5 mm. (B) Changes in the blood pressure during the experiments in each group. Values are expressed as mean ± SEM; n = 9–10 in each group.

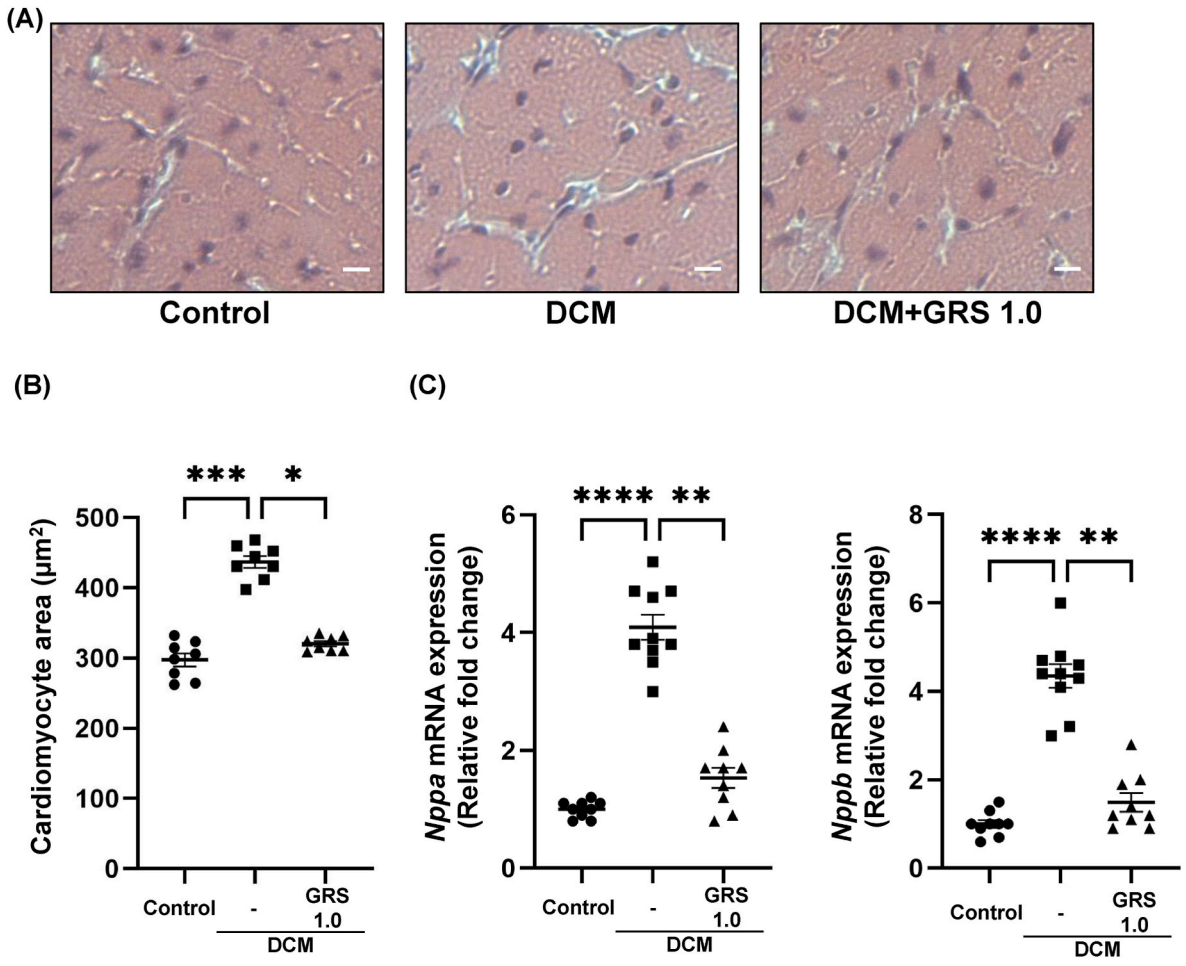

Fig. 2. Effects of GRS on cardiac hypertrophy in mice with DCM
(A) Representative histological images of hematoxylin and eosin (HE) staining of each group; scale bar: 10 μm. (B) Semi-quantitative analysis of cardiomyocyte cross-sectional areas; values are expressed as mean ± SEM; $^{*}P < 0.05$, $^{***}P < 0.001$, $n = 8$ in each group. (C) The mRNA levels of *Nppa* and *Nppb* in the heart are expressed as mean ± SEM. $^{**}P < 0.01$, $^{****}P < 0.0001$, $n = 8$ in each group.

addition, GRS was administered orally daily at a dose of 0.5 (GRS 0.5) or 1 (GRS 1.0) g/kg/day by water. Blood glucose (BG) levels were measured using the ACCU-CHEK Aviva kit (Roche Diagnostics, Basel, Switzerland). Blood pressure (BP) and heart rate were measured using a noninvasive computerized tail-cuff system (BP98A Softron Corp., Tokyo, Japan). Unanesthetized mice from each group were placed in a holding device mounted on a thermostatically controlled warming plate that was maintained at 37 °C. BP was measured on two consecutive days, and at least 10 readings were taken for each measurement. Serum total cholesterol (T-CHO) and triglyceride (TG) levels were determined by an enzymatic method (Oriental Yeast Co. Ltd., Tokyo, Japan).

2.3. Echocardiography

Echocardiography was performed using an F Jelly PLUS Ultrasound Gel, a 15–20 MHz probe, and a MyLab Sigma VET veterinary ultrasound imaging system. The left ventricular internal dimension in diastole (LVDd), left ventricular internal dimension in systole (LVDs), interventricular septal thickness in diastole (IVSd), and left ventricular posterior wall thickness (LVPWT) were measured using M-mode images. Fractional shortening (FS) was calculated using the following formula: FS = (LVDd - LVDs)/LVDd × 100 (%).

2.4. Histological analysis

Hematoxylin & eosin (HE) staining and picrosirius red (PSR) staining were performed as previously described.[12] The cardiomyocyte area, fibrotic areas surrounding the blood vessels and within the interstitial spaces were quantified using ImageJ 1.54d software.

2.5. Immunohistochemical staining and quantification of 4-HNE

Immunohistochemical staining for 4-HNE was performed on paraffin-embedded tissue sections. After deparaffinization, rehydration, and antigen retrieval, the sections were incubated with primary anti-4-HNE antibody at 4 °C overnight, followed by incubation with peroxidase-conjugated anti-rabbit immunoglobulin IgG (Histofine Simple Stain MAX-PO(R), Nichirei. Tokyo, Japan). The 4-HNE signal was visualized using the Peroxidase Staining DAB Kit (Brown Stain) (Nacalai Tesque) as a chromogen and counterstained with hematoxylin. To semi-quantify the extent of 4-HNE staining, the stained area in each image was measured using the ImageJ software. The percentage of the stained area relative to the total area of the image was calculated. Staining intensity was then categorized into four grades: rank 1 (0%–25%), rank 2 (25%–50%), rank 3 (50%–75%), and rank 4 (75%–100%). Five random microscopic fields per heart section were used for quantification using the ImageJ 1.54d software.

2.6. TUNEL staining

TUNEL staining was performed according to the protocol of the Apoptosis In Situ Detection Kit (FUJIFILM Wako Pure Chemical

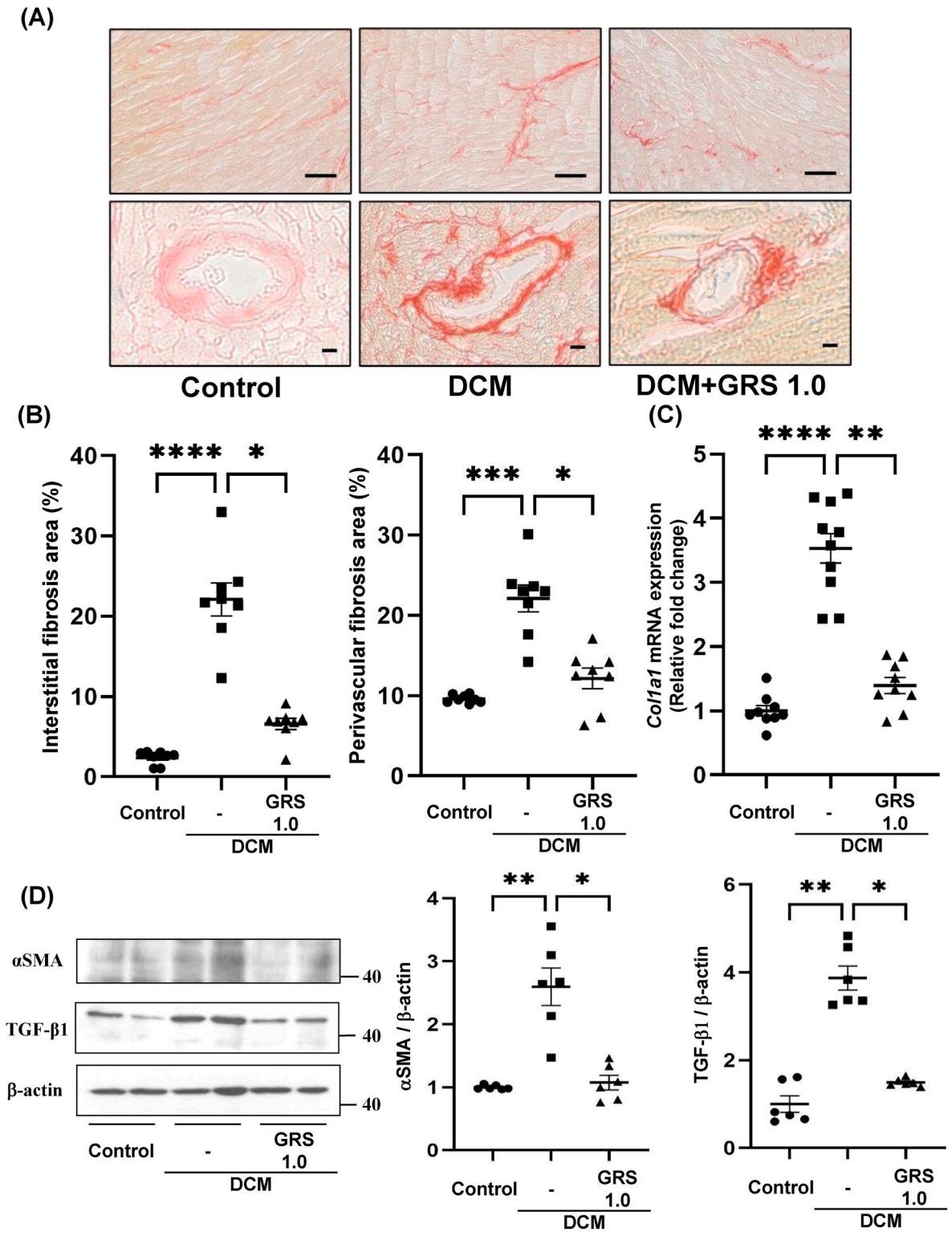

Fig. 3. Effects of GRS on cardiac fibrosis in mice with DCM
(A) Representative histological images of Picrosirius Red (PSR) staining in cardiac interstitial fibrosis (scale bar: 20 μm) and perivascular fibrosis (scale bar: 2 μm) in each group. (B) Semi-quantitative analysis of cardiac interstitial and perivascular fibrosis. Values are expressed as the mean ± SEM; $^{*}P < 0.05$, $^{***}P < 0.001$, $^{****}P < 0.0001$, $n = 8$ in each group. (C) The mRNA level of *Col1a1* in the heart is expressed as the mean ± SEM; $^{**}P < 0.01$, $^{****}P < 0.0001$,$n = 9$–10 in each group. (D) Protein expression of fibrosis-related genes. Left panel: Representative blots of TGF-β1 and αSMA, and β-actin. Right panel: Semi-quantitative analysis of TGF-β1 and αSMA corrected by β-actin. Values are expressed as mean ± SEM; $^{*}P < 0.05$, $^{**}P < 0.01$, $n = 6$ in each group.

Table 2
Echocardiogram parameters.

	Control (n = 9)	DCM (n = 10)	GRS 0.5 (n = 10)	GRS 1.0 (n = 9)
LVDd (mm)	2.64 ± 0.55	2.27 ± 0.10	2.28 ± 0.13	2.50 ± 0.10
IVSd (mm)	0.87 ± 0.02	0.80 ± 0.43	0.85 ± 0.30	0.94 ± 0.48
LVPWd (mm)	0.97 ± 0.48	0.87 ± 0.54	0.98 ± 0.67	1.00 ± 0.34
FS (%)	49.7 ± 1.9	33.3 ± 2.0*	38.5 ± 1.3	51.0 ± 1.4$^{\#}$
EF (%)	84.8 ± 1.5	68.7 ± 2.7*	67.3 ± 3.9*	88.3 ± 1.1$^{\#}$

Data represent mean ± SEM; $n = 9$–10; *$P < 0.05$ vs.control; $^{\#}P < 0.05$ vs. DCM. LVDd: left ventricular internal diameter in diastole, IVSd: interventricular septum thickness at end-diastole, LVPWd: left ventricular posterior wall dimension in diastole, FS: fractional shortening, EF: ejection fraction.

Table 3
Characteristics of each parameter.

	Control (n = 9)	DCM (n = 10)	GRS 0.5 (n = 10)	GRS 1.0 (n = 9)
Initial BW (g)	23.0 ± 0.23	22.4 ± 0.31	22.6 ± 0.38	22.3 ± 0.18
Final BW (g)	27.1 ± 0.31	19.5 ± 0.75*	20.4 ± 0.56*	23.4 ± 0.60*,$^{\#}$, $
Final HW (mg)	119 ± 1.8	93 ± 3.2*	95 ± 5.7*	110 ± 4.1
HW to BW ratio	4.4 ± 0.57	5.5 ± 0.22*	4.8 ± 0.19$^{\#}$	4.5 ± 0.12$^{\#}$
Final BG (mg/dl)	101 ± 4.2	341 ± 13.6*	367 ± 28.2*	367 ± 15.1*
T-CHO (mg/dL)	135.4 ± 5.7	295.1 ± 9.5*	ND	264.6 ± 10.3*
TG (mg/dL)	64.3 ± 3.3	99.8 ± 7.8*	ND	97.4 ± 13.1*

BW: body weight, HW: heart weight, BP: blood pressure, BG: blood glucose, T-CHO: total cholesterol, TG: triglyceride, ND: not done. Data represent mean ± SEM; $n = 9$–10; *$P < 0.05$ vs. Control; $^{\#}P < 0.05$ vs. DCM; $^{\$}P < 0.05$ vs. GRS 0.5.

Corporation, Osaka, Japan). After deparaffinization, the sections were treated with proteolytic enzymes at 37 °C for 30 min to increase tissue permeability. The sections were then incubated with the TUNEL reaction mixture containing TdT enzyme and labeled with dUTP at 37 °C for 60 min. Endogenous peroxidase activity was blocked with 3% hydrogen peroxide followed by incubation with a labeled antibody for 1 h. TUNEL-positive cells were visualized using the Peroxidase Staining DAB Kit (Brown Stain) (Nacalai Tesque) as a chromogen and counterstained with methyl green. After staining, the number of TUNEL-positive cells was counted, and the ratio of TUNEL-positive cells was calculated using the ImageJ 1.54d software.

2.7. RNA extraction and mRNA expression

RNA extraction, cDNA synthesis, and quantitative qRT-PCR were performed using commercially available reagents. The procedure was performed as described previously.[13] The primer sets used in this study are listed in Table 1.

2.8. Protein extraction and western blotting

Protein preparation and western blotting were performed as described previously.[14] Briefly, tissue samples were homogenized or sonicated in protein lysis buffer (RIPA buffer) containing protease and phosphatase inhibitors, and proteins were extracted. The extracted proteins were boiled for 5 min in the Laemmli sample buffer and used for western blotting. The immunoreactive bands were quantified by densitometric analysis using ImageJ 1.54.

2.9. Statical analysis

Data are presented as the mean ± standard error of the mean (mean ± SEM) with dot plots. Data were analyzed using one-way analysis of variance (ANOVA), followed by the Kruskal–Wallis test. Statistical significance was set at $P < 0.05$. Statistical analyses were performed using GraphPad Prism (version 9.5.1, GraphPad Software, San Diego, CA, USA). ns: not significant.

3. Results

3.1. Establishment of a new DCM mice model

Conventional DCM models require long periods of time and specific transgenic mice.[15] Moreover, the phenotype of previous DCM models is weak. Therefore, we aimed to establish a new DCM mouse model that was developed with a strong phenotype in a short time. Our model using HFD + STZ + L-NAME demonstrated a strong phenotype compared to the conventional model using HFD + STZ or L-NAME alone (Supplementary text and Figs. 1–3). Consequently, we used this model to examine the effects of GRS on DCM.

3.2. GRS suppresses cardiac dysfunction in DCM

First, echocardiographic assessment was performed to evaluate the effect of GRS on cardiac structure and function in DCM. FS was significantly reduced in the DCM group compared with the control group, while GRS 1.0, but not GRS 0.5, showed improved cardiac dysfunction compared with the DCM group (Fig. 1A and Table 2). The heart-to-body weight ratio was higher in the DCM group, but this was ameliorated by DCM with GRS 0.5 and GRS 1.0 groups. Fasting BG levels, as well as T-CHO and TG levels, were elevated in the DCM group, and there were no differences in BG levels among DCM, DCM with GRS 0.5, and DCM with GRS 1.0 (Table 3). The DCM group showed an increase in BP by week 4, and the elevated BP gradually decreased after STZ injection. There were no differences in BP changes between DCM groups, regardless of GRS administration. (Fig. 1B). GRS treatment ameliorated cardiac hypertrophy in DCM without affecting the BP, BG, T-CHO, and TG levels (Fig. 1A and Table 3). As cardiac dysfunction in DCM was inhibited by GRS 1.0 g/kg/day, further investigations were conducted using this dosage.

3.3. GRS inhibits cardiomyocyte hypertrophy in DCM

Cardiac hypertrophy was observed in DCM, as indicated by an increase in the heart-to-body weight ratio, which was inhibited by GRS. To investigate this further, HE staining was performed for histological analysis. The cardiomyocyte area increased in the DCM group, which was significantly suppressed in the GRS group (Fig. 2A and B). Similarly, elevated mRNA expression of *Nppa* and *Nppb* in DCM was suppressed by GRS treatment. (Fig. 2C).

3.4. GRS suppresses cardiac fibrosis in DCM

We evaluated the effect of GRS on cardiac fibrosis. Both cardiac interstitial and perivascular fibrosis were exacerbated in the DCM group but were mitigated by GRS administration (Fig. 3A and B). The expression of the fibrosis marker *Col1a1*, which was increased in DCM, was inhibited by GRS treatment (Fig. 3C). Similarly, the elevated expression of TGF-β1 and αSMA proteins in DCM was reduced by GRS treatment (Fig. 3D).

3.5. GRS suppresses oxidative stress and apoptosis in DCM

We examined the effects of GRS on oxidative stress and apoptosis in DCM. 4-HNE, a marker of lipid peroxidation, was elevated in DCM and was ameliorated by GRS administration (Fig. 4A–C). The mRNA expression of *Cyba* and *Cybb*, NADPH oxidase components, was

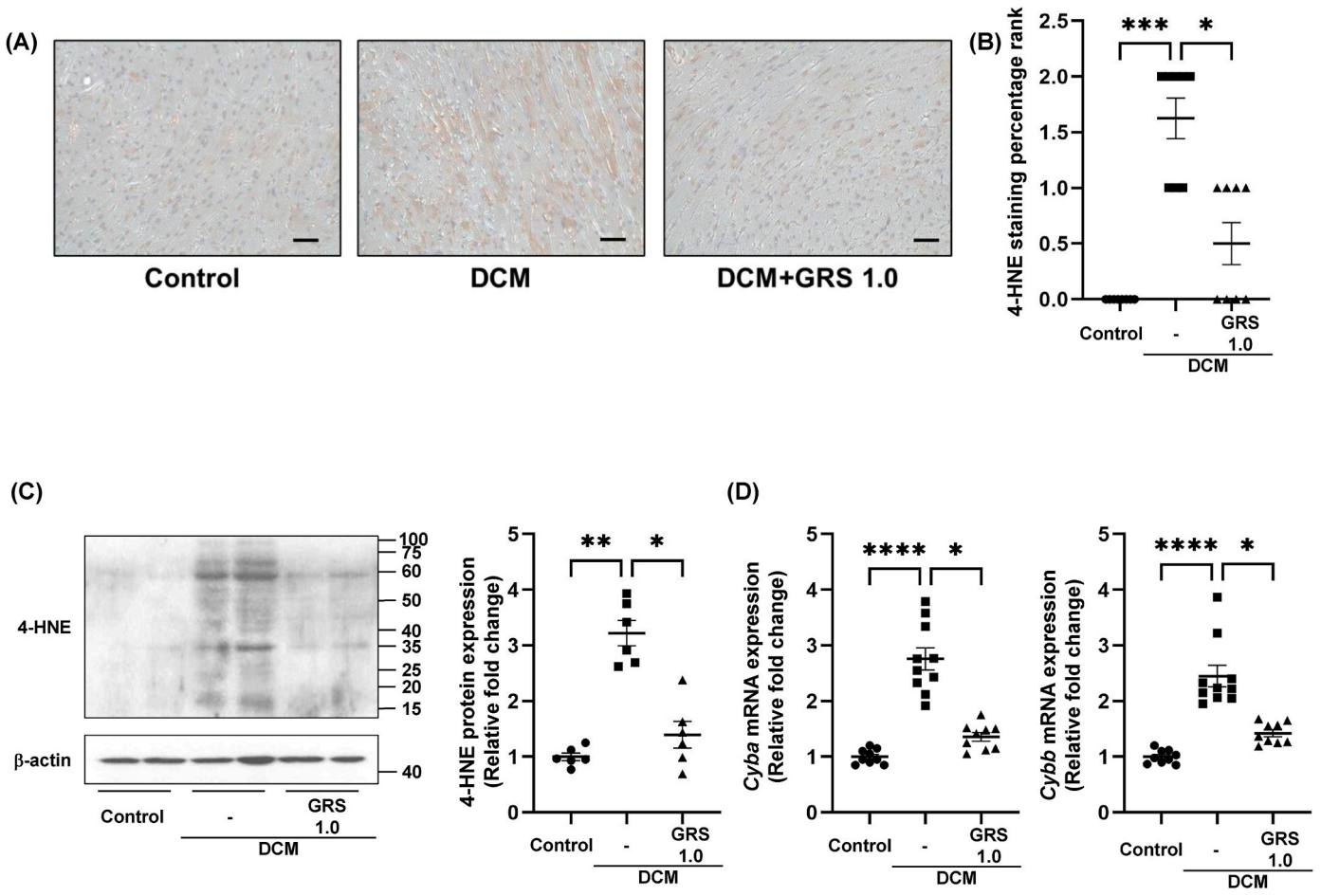

Fig. 4. Preventive effects of GRS against oxidative stress in DCM.
(A) Representative images of 4-HNE immunohistochemistry (scale bar: 20 μm). (B) Semi-quantitative analysis of 4-HNE grade scores in the control, DCM and DCM + GRS 1.0 groups. Values are expressed as mean ± SEM; $^{*}P < 0.05$, $^{***}P < 0.001$, $n = 8$ in each group. (C) Left panel: Representative blots for 4-HNE and β-actin. Right panel: Semi-quantitative analysis of 4-HNE corrected by β-actin. Values are expressed as mean ± SEM; $^{*}P < 0.05$, $^{**}P < 0.01$, $n = 6$ in each group. (D) mRNA levels of *Cyba* and *Cybb* in the heart are expressed as the mean ± SEM; $^{*}P < 0.05$, $^{****}P < 0.0001$, n = 9–10 in each group.

increased in DCM, but was inhibited in DCM with GRS treatment (Fig. 4D). TUNEL-positive cells and cleaved caspase-3 expression, which were elevated in DCM, were suppressed by GRS treatment (Fig. 5A–C). Additionally, Akt phosphorylation, a cell survival signaling pathway, was reduced in DCM and recovered with GRS treatment (Fig. 5C).

3.6. No effects of GRS on inflammatory cytokines in DCM

Although DCM mice showed increased expression levels of inflammatory cytokines, such as *Tnf*, *Il1b*, and *Il6*, these genes were not inhibited by GRS administration (Fig. 6).

4. Discussion

In this study, we established a new DCM mouse model that was developed over nine weeks. Using this DCM model, we found that GRS has a beneficial effect on DCM by inhibiting cardiac remodeling and dysfunction. GRS exerted anti-fibrotic, anti-oxidative stress, and anti-apoptotic effects, leading to the prevention of DCM development. In addition, GRS did not affect the diabetic condition and blood pressure; therefore, the effect of GRS in inhibiting the onset and development of DCM is independent of diabetes and blood pressure.

Numerous animal models of diabetes have been developed to replicate and mimic certain aspects of human DM, and several have been used to investigate the pathomechanisms of DCM. STZ induction, diet induction, STZ plus diet induction, and genetic modifications are major diabetes models used in DCM studies. The issue with these models is that they are time consuming, have a weak phenotype, and are reproducibility.[16] In the preliminary study, we examined the STZ model for 24 weeks; however, it had no or very weak phenotype of DCM, such as cardiac fibrosis (data not shown). Therefore, we attempted to establish a new DCM model in this study. This model mimics the clinical course of type 2 diabetes and has a definite onset of DCM with cardiac remodeling and dysfunction. Our model overcomes the above issues and is thought to be a very useful model for research on DCM.

GRS is composed of Alisma orientalis Juzep (Alisma plantago-aquatica L.), Polyporus umbellatus Fries (Polyporus umbellatus), Atractylodes chinensis (Atractylodes lancea), Poria cocos Wolf (Wolfiporia extensa) and Cinnamomom Cassia Presl (Cinnamomum cas-sia L. J. Presl).[12] GRS has diverse therapeutic applications, including reducing reoperation rates after burr-hole surgery for chronic subdural hematoma.[17] Its mechanisms of action, such as inhibiting vascular endothelial cell migration and angiogenesis, may explain its effectiveness in treating edema, headaches, and weather-related symptoms by regulating cerebral blood flow.[18,19] Additionally, GRS influences lymphatic pump function, which contributes to its diuretic effects and potential use in lymphedema treatment.[20]

DCM is characterized by cardiac remodeling, such as cardiac hypertrophy and interstitial fibrosis,[21] which eventually leads to heart failure. There are many pathogenic factors involved in DCM, and

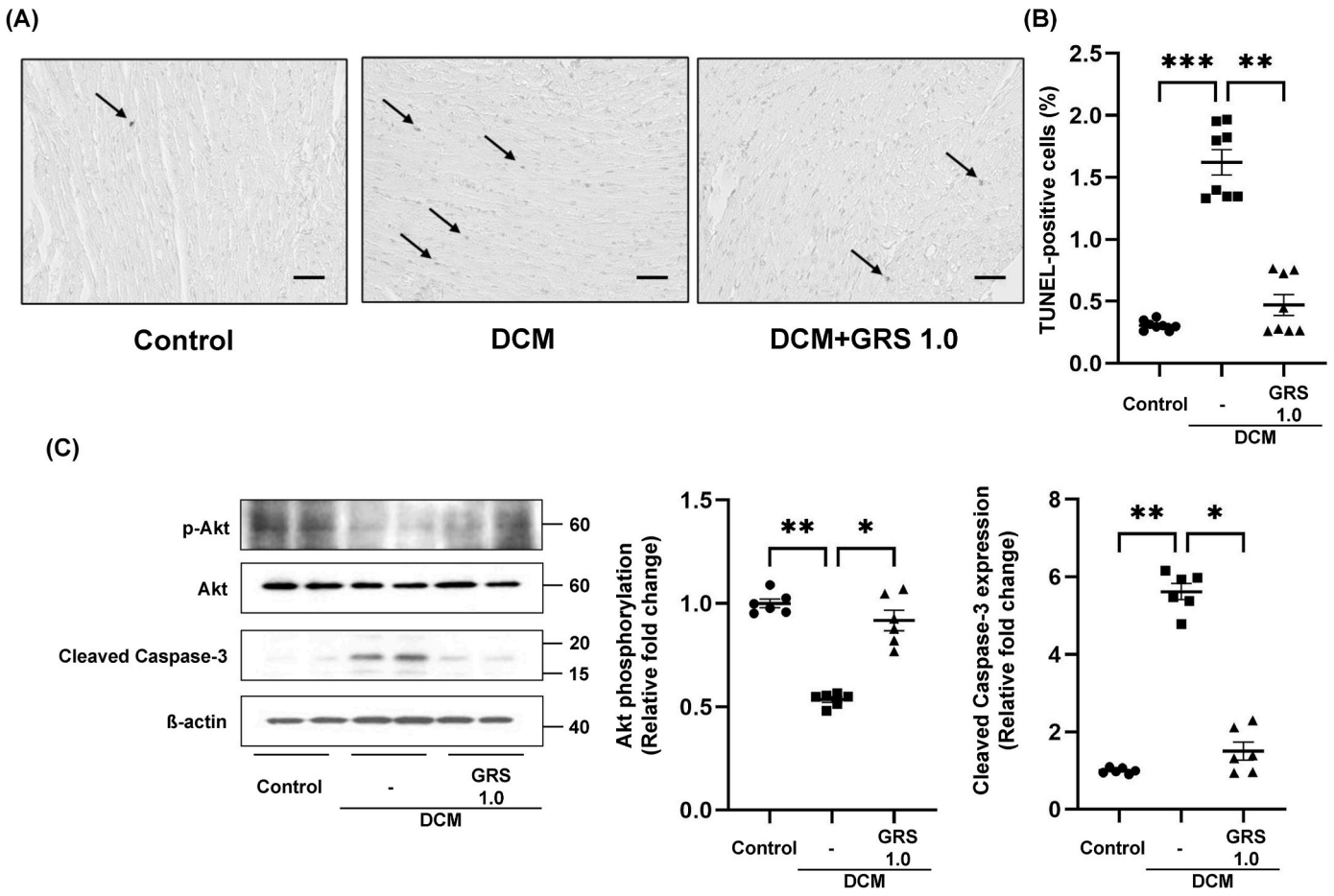

Fig. 5. Preventive effects of GRS against apoptosis in DCM.
(A) Representative images of TUNEL staining (arrows: TUNEL-positive cells; scale bar: 20 μm). (B) Comparison of the incidence of TUNEL-positive cells between the control, DCM and DCM + GRS 1.0 groups. Values are expressed as mean ± SEM; $^{****}P < 0.0001$, $n = 8$ in each group. (C) Left panel: Representative blots showing cleaved caspase-3, phospho-Akt, total-Akt, and β-actin levels. Right panel: Semi-quantitative analysis of cleaved caspase-3 corrected for β-actin and phosphorylation of Akt corrected for total Akt. Values are expressed as the mean ± SEM; $^{*}P < 0.05$, $^{**}P < 0.01$, $n = 6$ in each group.

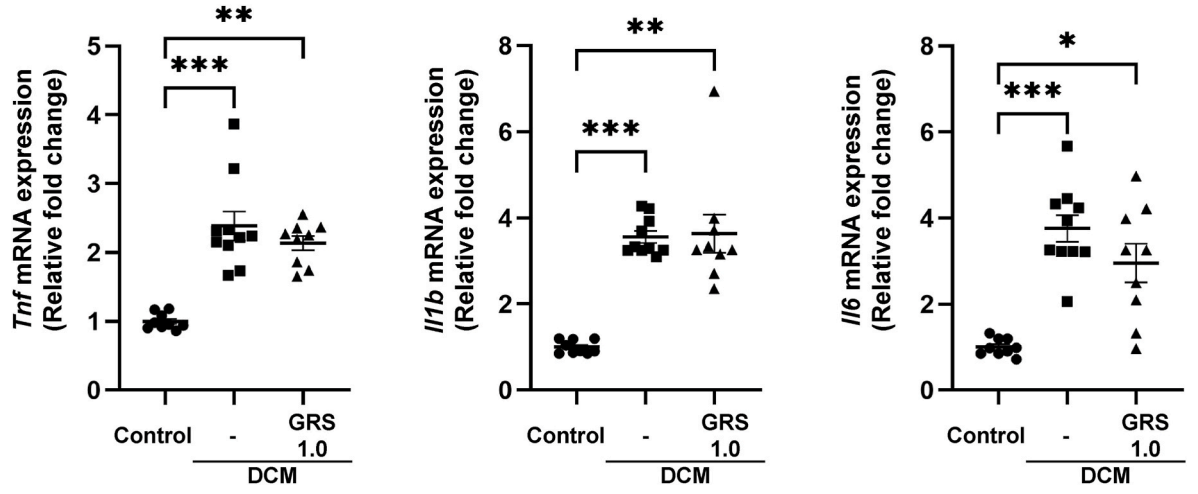

Fig. 6. No inhibitory effect of GRS against inflammatory cytokines in DCM
The mRNA expression of *Tnfa*, *IL1b*, and *Il6* in the heart of each group. Values are expressed as the mean ± SEM; ns: not significant, $^{*}P < 0.05$, $^{**}P < 0.01$, $^{***}P < 0.001$, $n = 9$–10 in each group.

oxidative stress is thought to be a crucial factor and a therapeutic target for DCM.[22] Our previous study revealed anti-oxidant properties of GRS against kidney injury.[12] In the present study, oxidative stress, including lipid peroxidation, increased in DCM, which was suppressed by GRS treatment.

Oxidative stress also induces cardiac fibrosis, contributing to

myocardial stiffening and dysfunction, and the inhibition of TGF-β and αSMA is critical for preventing fibrosis in heart.[23–25] In fact, we found that GRS attenuated the increased expression of TGF-β1 and αSMA in DCM. Oxidative stress is also a critical inducer of pathological cardiac hypertrophy, and therapeutic approaches using antioxidants may attenuate cardiac hypertrophy.[26] Markers of cardiac hypertrophy, such as HW-to-BW ratio, mRNA expression of *Nppa* and *Nppb*, and cardiomyocyte area, were elevated in the DCM model, but were ameliorated by GRS administration. In contrast, the heart weight decreased in DCM and was ameliorated by GRS. Diabetes increases the size of individual cardiomyocytes, which, on its own, could be anticipated to cardiac hypertrophy. At the same time, the total number of cardiomyocytes is reduced by apoptosis, which alone is expected to reduce heart weight.[27] Therefore, cardiomyocyte enlargement may occur to compensate for the loss of cardiomyocytes. Thus, the inhibitory effect of GRS on oxidative stress may contribute to the attenuation of two major pathways, cardiac hypertrophy and fibrosis, in DCM. DCM is characterized by increased oxidative stress, with NADPH oxidases playing a critical role in ROS production.[28] Indeed, we found that the mRNA expression of Cyba and Cybb was increased in DCM, which was alleviated by GRS treatment. Therefore, NADPH oxidase may be involved in the mechanism of action of GRS in oxidative stress in DCM. Further investigations are needed to clarify the detailed mechanisms underlying the preventive effects of GRS against oxidative stress.

GRS also suppressed apoptosis in DCM. Cardiomyocyte apoptosis leads to cell loss, which decreases cardiac contractile function and ultimately promotes cardiac remodeling.[29] Akt is a critical signaling pathway to regulate cell survival, growth, and metabolism.[30] In the heart, Akt also plays an essential role in supporting cardiomyocyte growth, proliferation, and survival.[31] In fact, Akt activation can have beneficial effects on cardiac injury and recovery in myocardial ischemia-reperfusion injury.[32] Akt has been reported to suppresses oxidative stress and apoptosis in cardiomyocytes, thereby improving myocardial remodeling.[33,34] Similarly to our findings, curcumin has been shown to attenuates apoptosis and enhances Akt phosphorylation in rat model with DCM.[35] Taken together, GRS inhibited apoptosis by enhancing reduced Akt phosphorylation, thereby contributing to myocardial dysfunction in DCM.

Inflammation plays a critical role in the pathogenesis of DCM. However, in this study, GRS failed to suppress inflammation in the hearts of DCM mice. GRS inhibits LPS-induced inflammatory cytokines in macrophages.[36] GRS also exerts an anti-inflammatory effect in kidney injury and autoimmune encephalomyelitis.[12,37] On the other hand, no effect of GRS on the inflammatory response in the intestine has been reported in an LPS-induced diarrhea model.[38] The effect of GRS on inflammation may be organ- or pathogenesis-dependent, and the preventive action of GRS on DCM appears to be independent of the inflammatory response. Further investigation is required to clarify this in the future.

5. Conclusion

GRS prevents the onset and development of DCM by inhibiting oxidative stress and apoptosis as well as suppressing cardiac remodeling and dysfunction. These findings indicate that GRS may be effective against DCM in diabetic patients.

CRediT authorship contribution statement

Masafumi Funamoto: Writing – review & editing, Writing – original draft, Investigation, Funding acquisition. **Shunji Hirose:** Writing – original draft, Investigation. **Mizuho Yamamoto:** Writing – review & editing, Investigation. **Hai Du Ly-Nguyen:** Writing – review & editing. **Masaki Imanishi:** Writing – review & editing. **Fuka Ebi:** Investigation. **Mai Ito:** Investigation. **Hirokazu Ohminami:** Writing – review & editing. **Koichiro Tsuchiya:** Writing – review & editing. **Yasumasa Ikeda:** Writing – review & editing, Supervision, Resources, Funding acquisition, Conceptualization.

Data availability

Data sharing is not applicable to this article, as no datasets were generated or analyzed during the current study.

Funding

This research was supported by a grant from Tsumura and Co., the 8th Japan Diabetes Foundation, and Nippon Boehringer Ingelheim Co., Ltd. & Eli Lilly Japan K.K. Research Grant, and the 3rd Japan Diabetes Foundation, Novo Nordisk Pharma Ltd. Research Grant.

Conflict of interest statement

The authors declare that the research was conducted without any commercial or financial relationships that could be construed as potential conflicts of interest.

Acknowledgments

We appreciate the excellent technical advice provided by the Support Center for Advanced Medical Sciences, Institute of Biomedical Sciences, Tokushima University Graduate School. We would like to thank Paperpal (https://paperpal.com/) for their help with English language editing.

Appendix A. Supplementary data

Supplementary data to this article can be found online at https://doi.org/10.1016/j.jphs.2025.01.003.

References

1. Funamoto M, Shimizu K, Sunagawa Y, et al. Effects of highly absorbable curcumin in patients with impaired glucose tolerance and non-insulin-dependent diabetes mellitus. *J Diabetes Res*. 2019;2019, 8208237.
2. Jia G, Hill MA, Sowers JR. Diabetic cardiomyopathy: an update of mechanisms contributing to this clinical entity. *Circ Res*. 2018;122(4):624–638.
3. Ritchie RH, Abel ED. Basic mechanisms of diabetic heart disease. *Circ Res*. 2020;126 (11):1501–1525.
4. Bugger H, Abel ED. Molecular mechanisms of diabetic cardiomyopathy. *Diabetologia*. 2014;57(4):660–671.
5. Lyon RC, Lange S, Sheikh F. Breaking down protein degradation mechanisms in cardiac muscle. *Trends Mol Med*. 2013;19(4):239–249.
6. Aneja A, Tang WH, Bansilal S, Garcia MJ, Farkouh ME. Diabetic cardiomyopathy: insights into pathogenesis, diagnostic challenges, and therapeutic options. *Am J Med*. 2008;121(9):748–757.
7. Cohn JN, Ferrari R, Sharpe N. Cardiac remodeling–concepts and clinical implications: a consensus paper from an international forum on cardiac remodeling. Behalf of an International Forum on Cardiac Remodeling. *J Am Coll Cardiol*. 2000;35 (3):569–582.
8. Dillmann WH. Diabetic cardiomyopathy. *Circ Res*. 2019;124(8):1160–1162.
9. Okayasu T, Mitani K, Kitahara T. Reviewing Kampo medicine (traditional Japanese herbal medicine) for otology/neurotology diseases. *Auris Nasus Larynx*. 2024;51(1): 25–30.
10. Jo M, Shibahara N. [Effect of Goreisan on the urinary concentrating ability and the expressions of aquaporins in 5/6 nephrectomized rats]. *Nihon Yakurigaku Zasshi*. 2014;143(2):65–68.
11. Yaku H, Kato T, Morimoto T, et al. Rationale and study design of the GOREISAN for heart failure (GOREISAN-HF) trial: a randomized clinical trial. *Am Heart J*. 2023; 260:18–25.
12. Suenaga A, Seto Y, Funamoto M, Imanishi M, Tsuchiya K, Ikeda Y. TJ-17 (Goreisan) mitigates renal fibrosis in a mouse model of folic acid-induced chronic kidney disease. *J Pharmacol Sci*. 2023;153(1):31–37.
13. Funamoto M, Sunagawa Y, Gempei M, et al. Pyrazole-curcumin suppresses cardiomyocyte hypertrophy by disrupting the CDK9/CyclinT1 complex. *Pharmaceutics*. 2022;14(6).
14. Funamoto M, Sunagawa Y, Katanasaka Y, et al. Histone acetylation domains are differentially induced during development of heart failure in dahl salt-sensitive rats. *Int J Mol Sci*. 2021;22(4).
15. Bugger H, Abel ED. Rodent models of diabetic cardiomyopathy. *Dis Model Mech*. 2009;2(9-10):454–466.

16. Jasińska-Stroschein M. The current state of preclinical modeling of human diabetic cardiomyopathy using rodents. *Biomed Pharmacother*. 2023;168, 115843.
17. Yasunaga H. Effect of Japanese herbal Kampo medicine goreisan on reoperation rates after burr-hole surgery for chronic subdural hematoma: analysis of a national inpatient database. *Evid Based Complement Alternat Med*. 2015;2015, 817616.
18. Murakami Ih K, Hara-Chikuma M, Shimizu Tomofumi, Matsumoto Chinami, Isohama Y. Goreisan regulates AQP3 expression and improves diarrhea. *Traditional & Kampo Medicine*. 2021;8(1):91–99.
19. Kurauchi Y, Ryu S, Tanaka R, et al. Goreisan regulates cerebral blood flow according to barometric pressure fluctuations in female C57BL/6J mice. *J Pharmacol Sci*. 2024;154(2):47–51.
20. Jo M, Trujillo AN, Shibahara N, Breslin JW. Impact of Goreisan components on rat mesenteric collecting lymphatic vessel pumping. *Microcirculation*. 2023;30(2-3), e12788.
21. Asbun J, Villarreal FJ. The pathogenesis of myocardial fibrosis in the setting of diabetic cardiomyopathy. *J Am Coll Cardiol*. 2006;47(4):693–700.
22. Byrne NJ, Rajasekaran NS, Abel ED, Bugger H. Therapeutic potential of targeting oxidative stress in diabetic cardiomyopathy. *Free Radic Biol Med*. 2021;169:317–342.
23. Cai L, Li W, Wang G, Guo L, Jiang Y, Kang YJ. Hyperglycemia-induced apoptosis in mouse myocardium: mitochondrial cytochrome C-mediated caspase-3 activation pathway. *Diabetes*. 2002;51(6):1938–1948.
24. Oruqaj G, Karnati S, Vijayan V, et al. Compromised peroxisomes in idiopathic pulmonary fibrosis, a vicious cycle inducing a higher fibrotic response via TGF-beta signaling. *Proc Natl Acad Sci U S A*. 2015;112(16):E2048–E2057.
25. Weber KT, Sun Y, Tyagi SC, Cleutjens JP. Collagen network of the myocardium: function, structural remodeling and regulatory mechanisms. *J Mol Cell Cardiol*. 1994;26(3):279–292.
26. Mohan M, Dihoum A, Mordi IR, Choy AM, Rena G, Lang CC. Left ventricular hypertrophy in diabetic cardiomyopathy: a target for intervention. *Front Cardiovasc Med*. 2021;8, 746382.
27. Ng HH, Leo CH, Prakoso D, Qin C, Ritchie RH, Parry LJ. Serelaxin treatment reverses vascular dysfunction and left ventricular hypertrophy in a mouse model of Type 1 diabetes. *Sci Rep*. 2017;7, 39604.
28. Hansen SS, Aasum E, Hafstad AD. The role of NADPH oxidases in diabetic cardiomyopathy. *Biochim Biophys Acta, Mol Basis Dis*. 2018;1864(5 Pt B):1908–1913.
29. Hu X, Bai T, Xu Z, Liu Q, Zheng Y, Cai L. Pathophysiological fundamentals of diabetic cardiomyopathy. *Compr Physiol*. 2017;7(2):693–711.
30. Shi X, Wang J, Lei Y, Cong C, Tan D, Zhou X. Research progress on the PI3K/AKT signaling pathway in gynecological cancer (Review). *Mol Med Rep*. 2019;19(6):4529–4535.
31. Aoyagi T, Matsui T. Phosphoinositide-3 kinase signaling in cardiac hypertrophy and heart failure. *Curr Pharmaceut Des*. 2011;17(18):1818–1824.
32. Matsui Y, Takagi H, Qu X, et al. Distinct roles of autophagy in the heart during ischemia and reperfusion: roles of AMP-activated protein kinase and Beclin 1 in mediating autophagy. *Circ Res*. 2007;100(6):914–922.
33. Fujio Y, Nguyen T, Wencker D, Kitsis RN, Walsh K. Akt promotes survival of cardiomyocytes in vitro and protects against ischemia-reperfusion injury in mouse heart. *Circulation*. 2000;101(6):660–667.
34. Matsui T, Li L, del Monte F, et al. Adenoviral gene transfer of activated phosphatidylinositol 3'-kinase and Akt inhibits apoptosis of hypoxic cardiomyocytes in vitro. *Circulation*. 1999;100(23):2373–2379.
35. Ren BC, Zhang YF, Liu SS, et al. Curcumin alleviates oxidative stress and inhibits apoptosis in diabetic cardiomyopathy via Sirt1-Foxo1 and PI3K-Akt signalling pathways. *J Cell Mol Med*. 2020;24(21):12355–12367.
36. Oh YC, Jeong YH, Ha JH, Cho WK, Ma JY. Oryeongsan inhibits LPS-induced production of inflammatory mediators via blockade of the NF-kappaB, MAPK pathways and leads to HO-1 induction in macrophage cells. *BMC Compl Alternative Med*. 2014;14:242.
37. Inada R, Miyamoto K, Tanaka N, Moriguchi K, Kusunoki S. Oryeongsan (goreisan) ameliorates experimental autoimmune encephalomyelitis. *Intern Med*. 2020;59(1):55–60.
38. Murakami K, Horie I, Isohama Y. Goreisan inhibits vascular endothelial cell migration and angiogenesis. *Traditional & Kampo Medicine*. 2021;8(1):83–90.